Structure of an active volcano associated with a resurgent block inferred from thermal mapping: The Yasur–Yenkahe volcanic complex (Vanuatu)

Aline Peltier, Anthony Finizola, G. A. Douillet, E. Brothelande, E. Garaebiti

Structure of an active volcano associated with a resurgent block inferred from thermal mapping: The Yasur–Yenkahe volcanic complex (Vanuatu)

A. Peltier [a,*], A. Finizola [b], G.A. Douillet [c], E. Brothelande [d], E. Garaebiti [e]

[a] Institut de Physique du Globe de Paris et Université Paris Diderot (Sorbonne Paris-Cité), UMR CNRS 7154—Géologie des Systèmes Volcaniques, 1 rue Jussieu, 75238 Paris cedex 05, France
[b] Laboratoire GéoSciences Réunion, Université de la Réunion, Institut de Physique du Globe de Paris (Sorbonne Paris-Cité), UMR CNRS 7154, 15 avenue René Cassin, BP 97715 Saint-Denis cedex 9, La Réunion, France
[c] Earth and Environmental Science Department, Ludwig-Maximilians-Universität München, Theresienstr 41, 80333 München, Germany
[d] PRES Clermont Université, Université Blaise Pascal, CNRS UMR 6524, Laboratoire Magmas et Volcans et IRD-R163, 5 rue Kessler, 63038 Clermont-Ferrand, France
[e] Vanuatu Meteorology and Geohazards Department, P.M.B 9054, Port Vila, Vanuatu

A B S T R A C T

Subsurface thermal measurements provide a valuable tool to map hydrothermal-fluid release zones in active volcanic areas. On the Yasur–Yenkahe volcanic complex (Tanna Island, Vanuatu archipelago), fumaroles and hot springs abound, signs of upraising heat fluxes associated to a well-developed hydrothermal activity. Com-bination of high resolution mapping of ground thermal anomalies with geomorphological analysis allows the characterization of the structural relationships between the active Yasur volcano and the Yenkahe resurgent block.
A complex system of heat release and hydrothermal fluid circulation below the Yasur–Yenkahe complex is evidenced. Circulation, though propagating vertically as a whole, is funneled by stratification. Thus, the main thermal fluid released is almost exclusively concentrated along structural limits that break the seals in-duced by the stratified nature of the ground. Three types of medium/high temperature anomalies have been evidenced: (1) broad hydrothermalized areas linked with planar stratification that favor lateral spreading,(2) linear segments that represent active faults, and (3) arcuate segments related to paleo-crater rims. The limit between the Yasur volcano and the Yenkahe resurgent block is characterized by an active fault system accommodating both the rapid uplift of the Yenkahe block and the overloading induced by the volcano weight. In such a setting, faults converge below the cone of Yasur, which acts as a focus for the faults. Evi-dence of such structures, sometimes hidden in the landscape but detected by thermal measurements, is critical for risk assessment of flank landslides.

1. Introduction

On active volcanoes, magma bodies at shallow depth may generate important heat fluxes by conduction and convection. At the surface, ground thermal anomalies coincide with permeable zones, where uprising hot fluids are preferentially released (Aubert and Baubron, 1988; Finizola et al., 2003; Lewicki et al., 2003; Chiodini et al., 2005; Aubert et al., 2007; Barde-Cabusson et al., 2009; Schöpa et al., 2011). Such areas can thus be mapped and monitored by aerial or ground thermal infrared pictures (Harris et al., 2000; Pergola et al., 2004; Harris and Ripepe, 2007; Lagios et al., 2007; Antoine et al., 2009; Delle Donne et al., 2010; Staudacher, 2010; Murphy et al., 2011) and/or by direct ground temperature measurements (Finizola et al., 2003; Lewicki et al., 2003; Aubert et al., 2007; Barde-Cabusson et al., 2009). Indirect thermal infrared measurements are subject to errors due to the distance between the object and the measurement point and thus need to be corrected; they depend upon surface emissivity of the object, background mixing of the signal, and atmospheric effects (Harris and Maciejewski, 2000). On the other hand, temperatures measured directly at the surface depend only upon the physical properties of the ground and the surface cover, and are affected by the climate (air temperature, wind, solar radiation, air humidity and rainfall). Surface temperatures thus fluctuate seasonally and daily and the surface heat is transferred in depth by conduction, though diurnal cycles generally vanish at one-meter depth. On Stromboli volcano, a diurnal amplitude of 1.1 °C has been measured at 30 cm depth in an area outside the thermal anomalies (Finizola et al., 2003). Thermal measurements carried out at several tens of centimeters below the surface thus minimize the effects of daily variations. In active volcanic areas, mapping the distribution and intensity of ground temperature anomalies allows to evaluate the extent of hydrothermal activity (Revil et al., 2004, 2008; Finizola et al., 2006; Lagios et al., 2007; Staudacher, 2010). Hydrothermal fluid circulation being the most efficient way to transfer heat from depth to the surface, subsurface thermal measurements provide a valuable tool to map fluid release

* Corresponding author.
E-mail address: peltier@ipgp.fr (A. Peltier).

zones, which are controlled by ground permeability and structural limits acting as preferential circulation paths.

The Yasur–Yenkahe volcanic complex (Tanna island, Vanuatu archipelago; Fig. 1A, B, C) exhibits consequent fumarolic activity as well as hot springs, signs of upraising heat fluxes associated to a well-developed hydrothermal activity (Gauthier et al., 2001). This volcanic complex is among the rare and most active association between (1) a volcanic cone with a persistent strombolian–vulcanian explosive activity, Yasur, to the west and (2) a rapidly uprising resurgent block, Yenkahe, to the east.

Even if the two structures (Yasur–Yenkahe) seem closely linked in regard to their location, the limits and the structural relationships between the two edifices remain poorly constrained. This study combines high resolution mapping of ground thermal anomalies with geomorphological analysis in order to characterize the structural relationships between the active Yasur volcano and the Yenkahe resurgent block.

2. Geological settings

The Yasur–Yenkahe volcanic complex is hosted within the Siwi caldera in the south-eastern part of the island of Tanna, which is part of the central chain of Vanuatu, related to the subduction of the Australian plate below the Pacific plate (Fig. 1A, B, C; Louat et al., 1988).

The Siwi caldera (9×4 km) hosting the Yasur–Yenkahe complex is delimited by the "Siwi Ring Fracture" on land (Fig. 1C; Carnay and Macfarlane, 1979), and extends offshore between Sulphur Bay and Port Resolution. The Yenkahe block, (6×3 km), is a resurgent block elongated N65 in the axis of the Siwi caldera. It is interpreted as formed

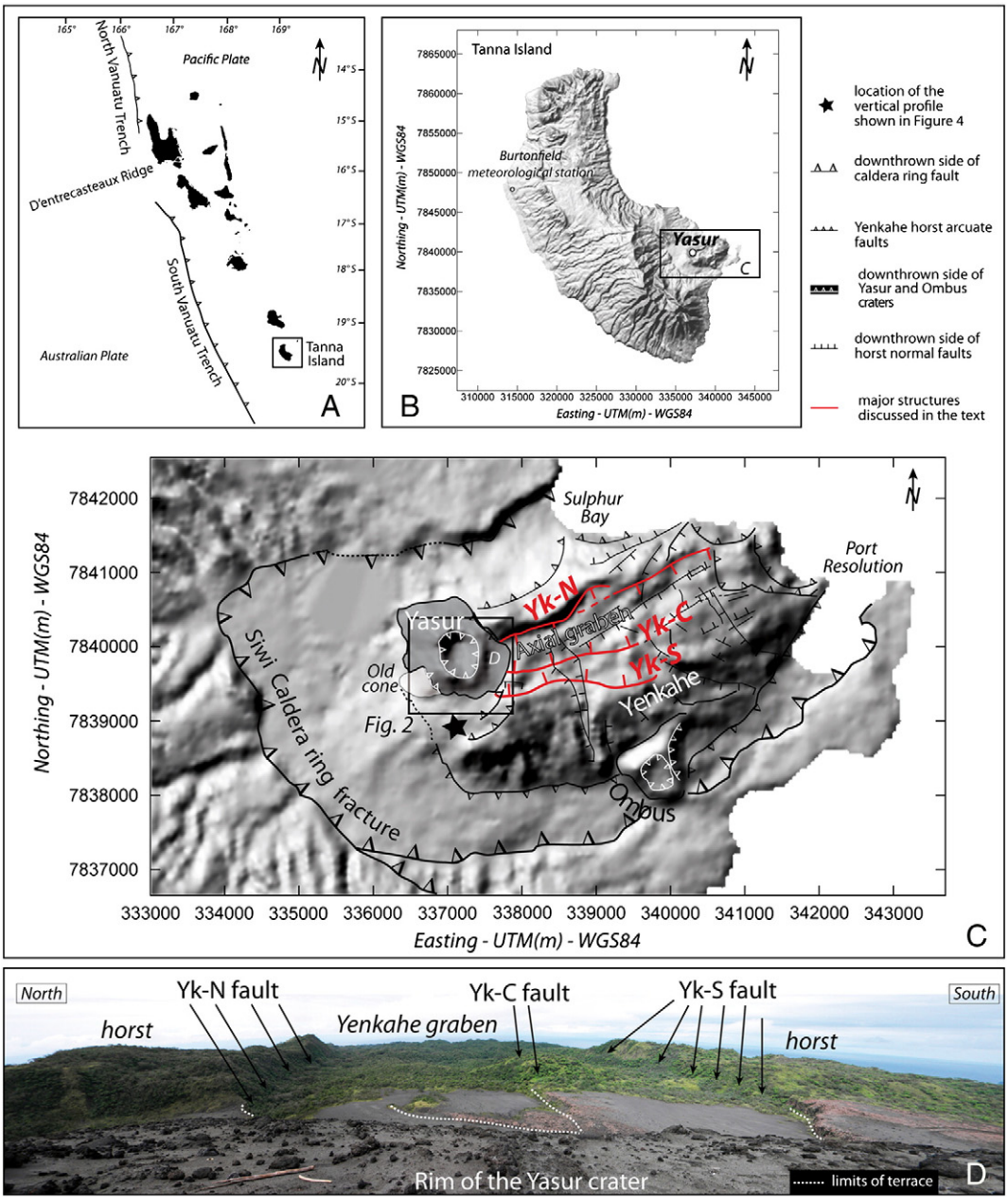

Fig. 1. A) Map of the Vanuatu archipelago and associated tectonic. B) Location of the Yasur–Yenkahe complex on the south-eastern part of the Tanna Island (SRTM digital elevation model). C) Structural map of the south-eastern Tanna including the Yasur–Yenkahe complex. D) Picture from the summit of Yasur to the east showing the main structures of the Yenkahe and the terraces at the junction between the two edifices.

by massive magmatic intrusions within the Siwi caldera (< to 20 ky; Nairn et al., 1988). Coral reef terraces dated at 1000 years BP are found at more than 150 m elevation, thus implying a mean uplift rate of 156 mm y^{-1} over the last millennium (Chen et al., 1995), whereas the regional uplift rate of the northern part of the island is around 1 mm y^{-1} (Chen et al., 1995; Neef et al., 2003; Taylor et al., 2005). GPS measurements carried out between 2002 and 2005 further indicate that the Yenkahe deformation is not continuous in time; periods of uplift and subsidence have succeeded one another, directly linked to the intrusive and eruptive activity (Erre, 2005). This consequent mean uplift rate recorded over the last millennium is at least partially controlled by local, catastrophic phenomena, such as earthquakes (e.g. the ones reported in 1878 and 1888 and responsible for a raise of the shoreline of about 20 m; Steel, 1880).

The Yenkahe structure is cut in its center by two main ENE–WSW parallel normal faults (Yk-N and Yk-S in Fig. 1C, D) that delimit an axial graben about 0.75 km wide. The axial graben extends to the west up to Yasur and is bordered to the north and to the south by two horsts extending almost along the full length of the block (Fig. 1C, D). On the northern, north-eastern (outside edge of the northern horst) and western edges of the Yenkahe block, numerous faults, several meters in throw, delimit terraces (Fig. 1D). The terrace sequences are associated to fumarole activity and altered material.

The normal fault pattern of the Yenkahe is consistent with an extensional deformation favoring dike injections along an EW axis (Rubin and Pollard, 1988). From the study of melt inclusions and volcanic gases, Metrich et al. (2011) estimate that 25 km^3 of magma have degassed without erupting and have accumulated beneath the Siwi caldera over the past 1000 years. Arcuate faults delimit the northern, eastern, and southern margins of the horsts (Fig. 1C). According to Nairn et al. (1988), these margins look like large slump scars, resulting from the massive uplift, rather than deep, nearly vertical, tectonic faults.

Yasur (361 m in height, 1500 m in diameter) is a permanently active volcano (at least since its first description in 1774, Aubert de la Rue, 1960) formed about 1400 year BP (Nairn et al., 1988). It is an unvegetated tephra cone lying on the western edge of the Yenkahe block. A 400 m wide crater, with three active vents is located in the summit (Fig. 2). The current active cone is partially hosted within the remnants of an older cone still outcropping to the south–west (Fig. 1C). The latter forms a steep sided and sharp semi-circular crest with a surface exhibiting indurated ash and lapilli layers with subplanar stratification, following the steep flank, as well as various colors of alteration. On the outer flank, hot clay material can be found associated with fumaroles and sulfur deposits. To the north, evidences of this older structure disappear below recent ash deposits.

3. Methods

A high-resolution mapping of ground thermal anomalies has been performed to image and characterize the structural relationship between the Yasur cone and the Yenkahe block.

Subsurface temperature measurements were carried out during a field campaign spanning between July 28th and August 14th 2011. Forty-six east–west profiles were made on an area covering 1300 × 1125 m (Fig. 2), extending from the summit to the base of the cone, up to the limit of vegetation (to the east and the south) or up to steep cliffs (to the west). No measurement was made on the northern and north-western flanks due to the almost constant gas plume in this direction, and sometimes falling bombs, representing a threat for scientists. The profiles are spaced 25 m apart, and temperature measurements were acquired every 10 m along the 46 profiles.

Ground temperature was measured at a depth of 30 ± 1 cm. K-type thermal probes were inserted in holes burrowed with a 2 cm diameter steel rod and subsequently filled and compacted. After the probes were left 15 min in the ground in order to achieve thermal equilibrium, the measurements were acquired with a digital thermometer (0.1 °C sensitivity).

In order to assess and correct the temperature variations linked to the rainfall events and water infiltration in the ground, a profile (see Fig. 2 for location) was re-iterated 8 times during the field campaign

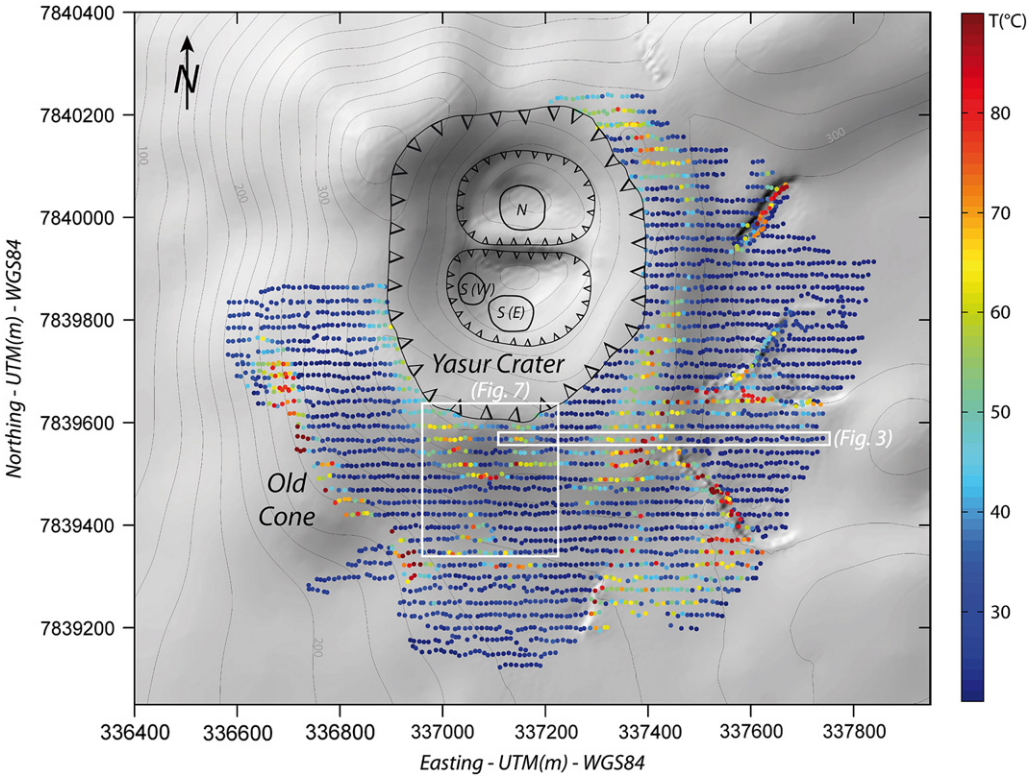

Fig. 2. Temperature measurements on the Yasur cone superimposed on a digital elevation model. (DEM: courtesy of M. Chaput; Chaput, 2009).

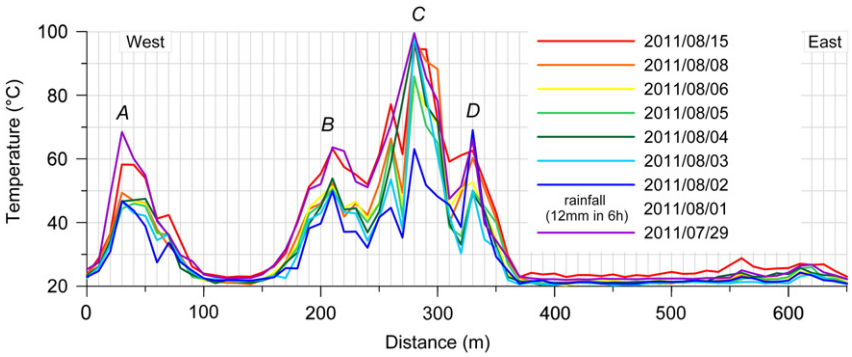

Fig. 3. Temperature along the re-iteration profile. See Fig. 2 for location.

(Fig. 3). This profile covered the whole temperature range of the studied area. The reference curve was measured on July 29th, under dry condition. Empirical best-fit curves plotted between the reference curve and the re-iterated ones were used to adjust the temperature cooled by rainfall infiltration effects. The corrected temperature data was then interpolated by a two steps krigging (13 m then 6 m grid spacing), according to the procedure described in Finizola et al. (2002).

4. Results

4.1. Vertical profile

In order to investigate the influence and the control of the vertical lithological variation on the hydrothermal fluid propagation, temperature was measured along a vertical profile. The vertical profile is located

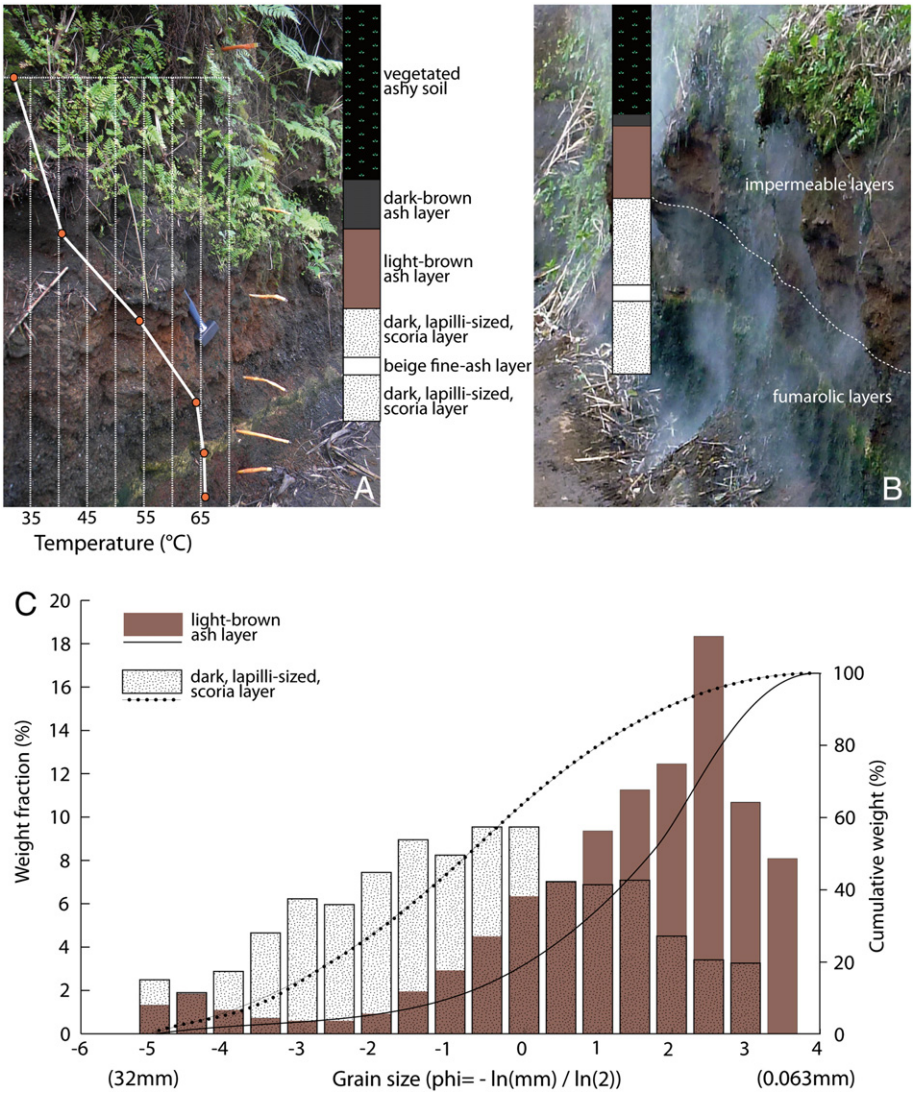

Fig. 4. Vertical profile (see Fig. 1 for location). A) Picture of the vertical profile and the associated temperatures. The compositions of distinct layers are shown as geological log. B) Picture showing the fumaroles at the base of the outcrop. C) Grain size distribution of the scoria permeable layer and of the ashy impermeable layer. (For interpretation of the references to color in this figure legend, the reader is referred to the web version of this article.)

about 800 m south of the Yasur crater (see Fig. 1C for location), where the road cuts into the ground, producing an 8 m high cliff. The outcrop exhibits planar stratification dipping to the east (Fig. 4A). The base (road level), from which fumaroles originate, consists of two, 40 cm thick, massive layers of dark, lapilli-sized, scoria, with a 8 cm thick, beige layer of fine-ash intercalated (Fig. 4B). These layers, partly colored in red, are altered. They are covered with an unsorted, light-brown, ash layer about 50 cm thick and a dark-brown layer of approximately same grain size. Ash, organic material, and roots forming a soil make the upper part of the outcrop. Grain-size analysis was carried out on 400 g samples from the upper scoria layers and the immediately surrounding, topping, light-brown, ash layer. Median diameter (Md) and sorting value (σ; Otto, 1939) were calculated from cumulative-weight curves obtained from interpolated discrete sieving results (Fig. 4C). The layer from which fumaroles blew ($Md = -0.7\ \Phi$; $\sigma = 2.1\ \Phi$) is much coarser-grained and less sorted than the overlying one ($Md = 1.7\ \Phi$; $\sigma = 1.6\ \Phi$).

For the vertical temperature profile, the thermal probes were inserted in the ground perpendicularly to the outcrop plan. Six measurements were taken within the first meters of the outcrop (one within each distinct layer; Fig. 4A) and another one 5 m higher. The temperature is stable at 64–65 °C within the two basal scoria layers and intercalated beige fine-ash layer, but decreases upward; at 54.3 °C in the light-brown ash layer, and 40.7 °C and 32.1 °C at 20 and 60 cm from the light-brown layer, respectively, vanishing to 28.8 °C on the upper part of the outcrop at ~5 m from the base.

4.2. Re-iterated profile

During the field campaign, only one day of consequent rainfall occurred (12 mm recorded in 6 h on August 1st 2011 at Burtonfield Tanna meteorological station, see location in Fig. 1B). The re-iterated profile shows the effect of the rainfall on August 1st 2011 on the ground temperature (at 30 cm depth; Fig. 3). Rainfall disturbed the measurements on the re-iteration profile up to several tens of degrees with a heterogeneous impact both in time and space. The re-equilibrium duration of the temperature values to those observed before the rainfall is distinct all along the profile. Two kinds of anomalous temperature peaks can be distinguished on the profile: (1) "medium temperature anomalies" ($60 < Tmax < 70$ °C; "A", "B", and "D" in Fig. 3) and (2) "high temperature anomalies" ($Tmax > 95$ °C; "C" in Fig. 3). For the "medium temperature anomalies", the temperature re-equilibrium was obtained in about 15 days, whereas for the "high temperature anomaly", re-equilibrium was achieved within only 2 days.

The data of the re-iterated profile was systematically used after the August 1st rainfall to correct temperatures of infiltration effects. The corrections (see the method section) allow us to correlate on a same map all measurements made during the 18 days of field campaign.

4.3. High-resolution ground temperature map

A total of 2992 thermal measurements were performed (Fig. 2) to produce a high-resolution, interpolated map of ground temperature (Fig. 5A). The data set was analyzed through a statistical analysis, the probability plot technique (Sinclair, 1974), generally used in volcanology for soil diffuse degassing measurements (Chiodini et al., 1998; Carapezza et al., 2009). The results show 3 inflection points suggesting 4 distinct populations of temperature ranges ("cold temperature anomalies", "low temperature anomalies", "medium temperature anomalies", "high temperature anomalies"; Fig. 6A). The coldest values (<21.3 °C; 8.1% of the data set; Fig. 6A, B) correspond to vegetated areas (at the limit of our studied area) or to areas with erosive and drainage structures, guiding streams of water on ground surface.

The largest population, 79.6% of the data, corresponds to "low temperature anomalies" ($21.3 < T°C < 58.8$) and can be considered as the background temperature of the studied area.

The "medium" ($58.8 < T°C < 95.9$) and the "high temperature anomalies" ($95.9 < T°C < 99.6$) are distributed on specific areas. Regarding their spatial distribution and the associated geomorphological expressions, three types of "medium (and high)" anomalous temperature areas can be highlighted (Fig. 5A, 6C): (1) linear segments near the base of the cone (mainly to the east of the studied area), (2) arcuate segments around the summit of the cone, and to the south-west, and (3) broad anomalous areas to the south.

(1) The linear segments of medium anomalous temperature are spatially distributed at the junction between the Yasur cone and the Yenkahe resurgent block. Six linear segments can be followed on the temperature map (F-N, F-NE, F-E, F-SE, F-SSW, F-SW; Fig. 5). Their temperatures range between 58.8 and 99.6 °C, including thus the "high temperature anomalies" population (Fig. 6C).
These segments are associated with clear geomorphological expressions consisting of cliffs in the continuation of the horst and graben at the junction between Yasur and Yenkahe (Figs. 1D, 5A, B). Most of the hottest points of these linear segments (85°–99.6 °C) are measured along the two cliffs with fumaroles (F-N and F-SE). These cliffs are in continuity with the western end of the northern and southern edges of the two horst-structures of Yenkahe, delimitating the central graben (Yk-N and Yk-S in Fig. 1C, D). A third segment, orientated NE-SW (F-NE on Fig. 5B), is sub-parallel to the northern cliff. The latter joins with another segment (F-E) in the continuation of the small mount in the middle of the Yenkahe graben (Yk-C). Two other segments are associated with smaller cliffs (1 to 3 m in throw; F-SW, F-SSW) and minor fumaroles.

(2) Four arcuate segments of medium anomalous temperature can be distinguished around the summit (Ys-NE, Ys-E, Ys-SE, Ys-S; Fig. 5) and three in the south-western part of the study area, at the base of the cone (OYs-W, OYs-SW and OYs-S; Fig. 5A). A temperature of 94 °C has been measured in sulfur precipitates found along the OYs-S segment at the base of the cone.
These anomalies underline small crests visible in the geomorphology. A close inspection of the thermal measurements allows distinguishing the diffuse contours of these features in the measurements. Although the thermal maximum for each arcuate structures is located on the outer flank of the topographical crests, the expansion limit of the abnormal high-temperature coincide with the crest (Fig. 5A).

(3) The broad anomalous areas display the lowest "medium" anomalies (<80 °C) and correspond to zones where altered and argilized sub-planar stratification outcrops (AA-S, AA-SE; Fig. 5).
AA-SE exhibits altered, relatively fine-grained and indurated, sub-horizontal stratification on the surface. It corresponds to ancient pyroclastic deposits emplaced by fallout that have been buried and subsequently exhumed. The northern edge of this area is outlined by a sub-vertical step, with a 2–3 m throw. AA-S displays a triangular shape (Fig. 5A). Its geomorphological expression consists of a slightly sur-elevated surface of altered material with sub-planar laminations parallel to the flank. The western limit of this structure is a radial erosive gully at the limit with the old cone, from which consequent fumarolic activity, with formation of sulfur crystals, is observed (at the southern end of OYs-S, Fig. 5A).

5. Discussion

Subsurface thermal measurements allow to image hydrothermal-fluid release zones. In the following, we discuss (1) the influence of water infiltration during rain events on subsurface temperature anomalies, (2) the modalities of thermal fluid circulation in regard to the geological context,

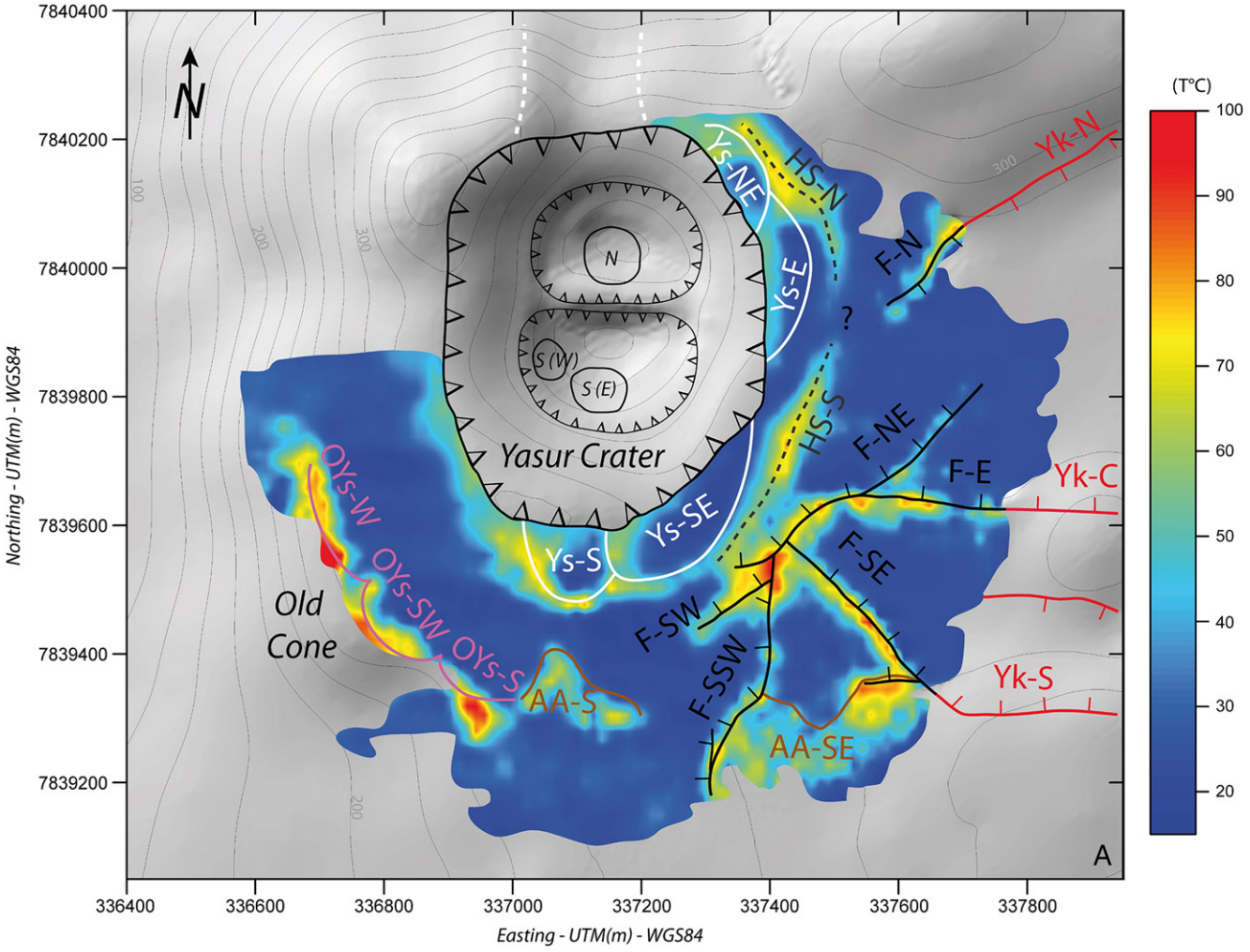

Yasur cone	current crater rim	crater rim
	argilized area limit	recent flank sliding border
	structural limit deduced from thermic map	
Old cone	crater rim	
Yenkahe	normal fault	

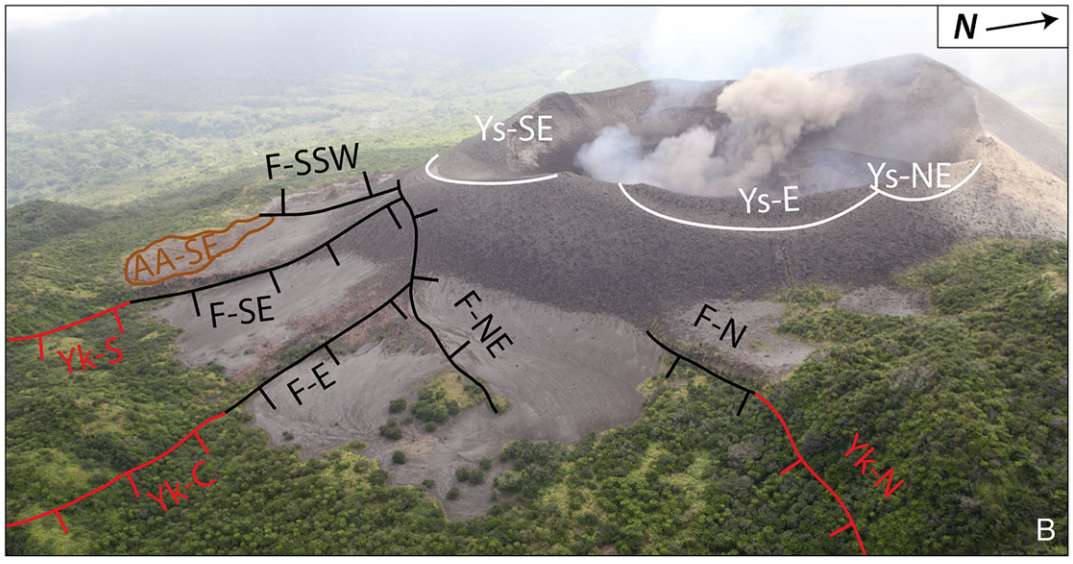

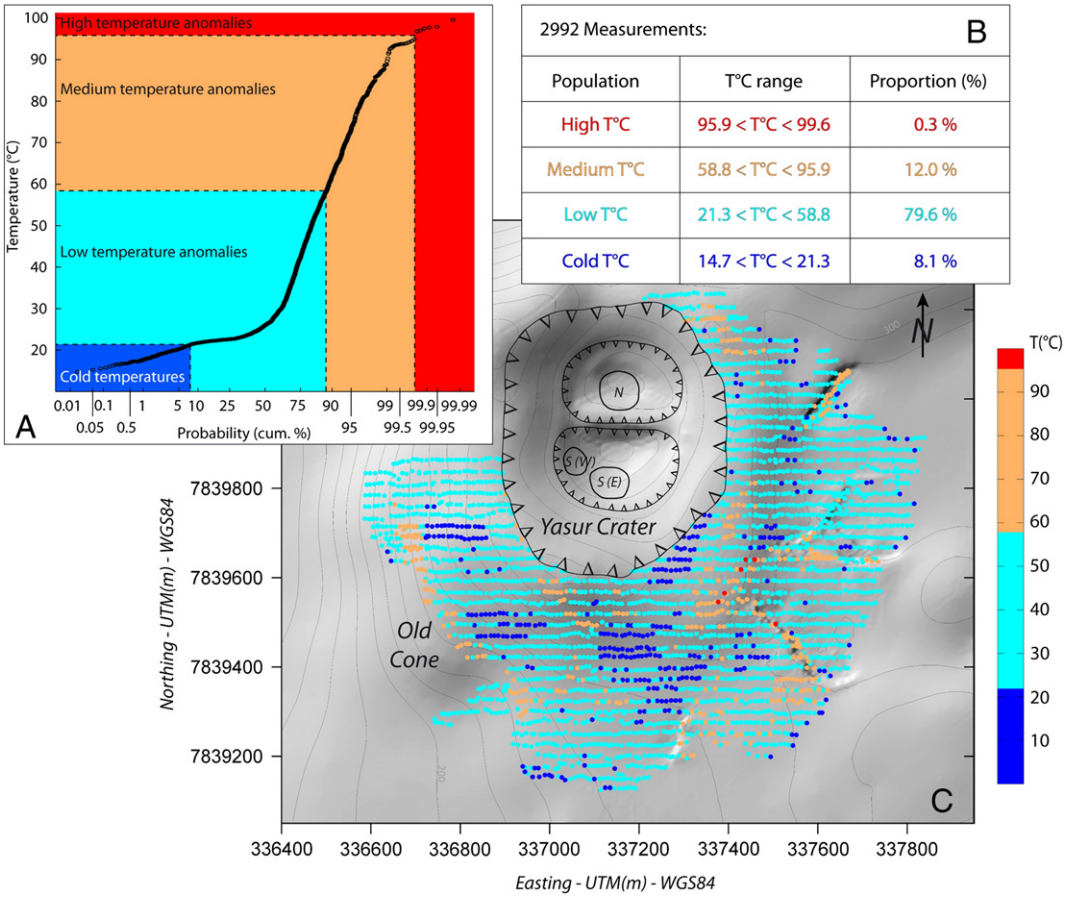

Fig. 6. A) Probability plot of the temperature data set. B) Temperature range and proportion of each population deduced from the probability plot. C) Temperature distribution according to their population type evidenced on the probability plot superimposed on a digital elevation model. (DEM: courtesy of M. Chaput; Chaput, 2009).

(3) the interpretation of anomalies evidenced on the Yasur–Yenkahe complex, and the implications for their structural relationship, and (4) the threat of weakness zones for local population and tourism.

5.1. Ground temperature variation linked to meteoritic water infiltration

The diverging response-time of anomalous temperature peaks of the re-iterated profiles to the rainfall disturbance (Fig. 3) can be interpreted in terms of heat-flux intensity: the shortest re-equilibrium duration, the more influent the heat flux. Thus, the "high temperature anomalies" (close to the boiling point of water at the subsurface) with the shortest re-equilibrium duration drag much more energy (by convection) than the "medium temperature anomalies" (below the boiling point of water at the subsurface) that needed ~15 days to return to pre-rainfall temperatures. It can therefore be considered that greater heat fluxes reach the surface for the "high temperature anomalies" than for the "medium" ones. The discrepancy in time-response can also be explained by considering that the "high" temperatures are most likely related to more permeable zones guiding hydrothermal fluid circulation more efficiently.

Our repeated temperature measurements clearly show the influence of rainfall events on the shallow temperature. As a consequence, meteoric aspects are rather critical to assess heat transfers deduced from infrared images interpretation. As shown in the context of the Yasur volcano, subsurface temperatures can be quantitatively analyzed only with a good knowledge of the climate (pluviometry, …) and its influence on the sub-surface temperatures.

5.2. Fluid circulation within the geological context

Most of the "medium/high thermal anomalies" are linked with clear geomorphological expressions. Three types of settings are found to be linked with hydrothermal fluid circulation at the surface: 1) broad altered zones with sub-planar stratification, 2) visible fault planes concentrating fluid releases and associated with consequent alteration and fumaroles, and 3) arcuate structures with a topographic expression but covered with recent scoria.

5.2.1. Effect of stratification on fluid circulations

Along the vertical profile, the high temperatures and fumarolic activity are confined in the coarse-grained, and thus more permeable, layers and the temperature vanishes upward in the finer grained layers (Fig. 4A, B). The fine-grained covering layers thus act as a seal and the hydrothermal fluids were trapped in the coarse-grained layers, where they could easily propagate laterally. Thus, even if the general tendency of hydrothermal fluids is to move upward, most of the transfers are made laterally, as long as the seal is not broken. This is further supported by previous observations where hydrothermal fluids were found to propagate parallel to the surface (e.g. Finizola et al.,

Fig. 5. A) Temperature map of the Yasur cone and associated structures superimposed on a digital elevation model. (DEM: courtesy of M. Chaput; Chaput, 2009). B) Aerial photo of Yasur (courtesy of Clémentine Bacri and Adrien Normier, ORA association). "OYs", "Ys" and "Yk" stand for Old Yasur, Yasur and Yenkahe, respectively. "AA", "F", and "HS" stand for Argilized Area, Fault and Hidden Structure, respectively.

2010; Revil et al., 2011). Stratification thus plays a major role in controlling the vertical versus horizontal propagation of hydrothermal fluids.

This prominence of lateral fluid transfers is illustrated by the two broad hydrothermalized anomalous areas (AA-S and AA-SE, to the south and to the south–east, respectively; Fig. 5). The broad distribution of these anomalies is linked to the stratified nature of the undergrounds that favors lateral propagation of hydrothermal fluids. The layers were permeable enough to permit vertical propagation, but the stratification as well as the clay produced by the consequent alteration tends to increase lateral propagation and spreading of hydrothermal fluids. Thus, where no break in the stratification is present and the lamination is sub-planar, hydrothermal fluids tend to diffuse on a broad zone rather than purely vertically. Since fluids are spreading on a broad zone, the anomalies are not as sharply defined and are lower in intensity (<80 °C) than for segments concentrating the hydrothermal releases.

On the whole, the entire Yasur cone is affected by such lateral heat propagation (at various degree of intensity). Fig. 6C shows that the background temperatures of Yasur are not cold but coincide with "low temperature anomalies (21.3<T°C<58.8). This is directly related to the shallow depth of the heat sources (Lardy and Tabbagh, 1999) and the nature of the volcanic environment, which allow a large diffusion of uprising fluids. This is supported by the DC-electrical resistivity tomography (Chaput, 2009) showing a continuous conductive body of about 2–60 Ω m and interpreted as a clay level, at 100–150 m depth below the surface.

5.2.2. Structural limits

5.2.2.1. Faults. The high-temperature linear segments associated with cliffs correspond to the throws of normal faults at the junction between Yasur and Yenkahe. The F-N and F-SE faults have the highest throws (~15 m). These two faults, in the continuity of the Yk-N and Yk-S faults delimiting the axial graben, most probably correspond to the termination of the Yenkahe structures on the resurgent block.

All linear faults seem to converge toward a point south–east of the crater (X ~337410, Y ~7839560; WGS84 coordinates; Fig. 5A). The convergence is clear in the landscape for the F-SSW, F-SE, F-E and F-NE faults, whereas no sign of convergence is visible in the surface for the F-N fault, since the faults get covered and vanish below the scoria cone. The Yasur cone, which grew in the western end of the Yenkahe graben, thus seems to capture these converging faults. The overloading produced by the Yasur edifice locally changes the regional stress field, such that faults are re-oriented below the cone and that the tensional component of pre-existing faults increases as observed on the thermal map (Fig. 5A). Indeed, in such an extensive area, models have shown that faults would curve toward the volcanic edifice, forming "hour-glass" patterns if a ductile layer is present (vanWyk de Vries and Merle, 1996, 1998). Such patterns are also observed at Fieale volcano, Axial and Brown Bear seamounts and Maderas volcano (vanWyk de Vries and Merle, 1996).

Except one point (measured along the F-SE fault in a fumarole; Fig. 6C), the "high temperature anomalies" are found close to the intersection of the linear faults (at the junction between the F-SSW, F-SE and F-NE faults; Figs. 5A, 6C). This intersection point is thus a major structure of the Yasur–Yenkahe complex with preferential uprising fluid releases.

As a whole, the junction between the Yenkahe resurgent block and the Yasur volcano is a highly active and faulted zone. This feature shows that active deformation occurs and is accommodated by brittle faults.

5.2.2.2. Paleo-crater rims. The arcuate structures correspond to paleo-crater rims that have been subsequently refilled.

Three arcuate high-temperature segments are visible to the south-western limit of the map (OYs-W OYs-SW OYs-S; Fig. 5A). They correlate in the field with the major geomorphological expression corresponding to the limit of the older and bigger cone, on which Yasur has built (Nairn et al., 1988). These segments, though not continuous, are probably part of the same structure. Indeed, the older cone is cut by erosive gullies that produce the topographical and thermal separation but the whole is made of the same indurated ash and lapilli layers with subplanar stratification following the steep flank and various colors of alteration. Additionally, the southern broad anomalous area (AA-S) might also be a remnant of the older cone, since it is made of the same material with stratification planes parallel to the outer steep flanks and it is in line with the three arcuate segments. However, a local drainage basin covered in recent scoriaceous material separates the broad anomalous area from the rest of the structure and inhibits conclusion on their link.

5.2.2.3. Hidden structures. Two segments of the thermal map (HS-N and HS-S; Fig. 5A) cannot be associated with any geomorphological features. We interpret these two segments as hidden structures, covered by recent, ashy-lapilli, scoriaceous material, and linked in depth to permeable zones.

Regarding their location, two hypotheses can be advanced concerning their origin:

1) The HS-N and HS-S structures could be linked and underlain one unique bigger paleo-crater rim. This large crater boundary could explain why the small craters, inside it (Ys-SE, Ys-E and Ys-NE), do not drag more uprising fluids up to the surface, as all the other structural boundaries of the Yasur cone do. Indeed, there is a shift between the temperature maximum and the smallest crater rims (Ys-SE, Ys-E and Ys-NE). Considering HS-N and HS-S as a big crater, the arched crater rim faults of this latter would be rooted

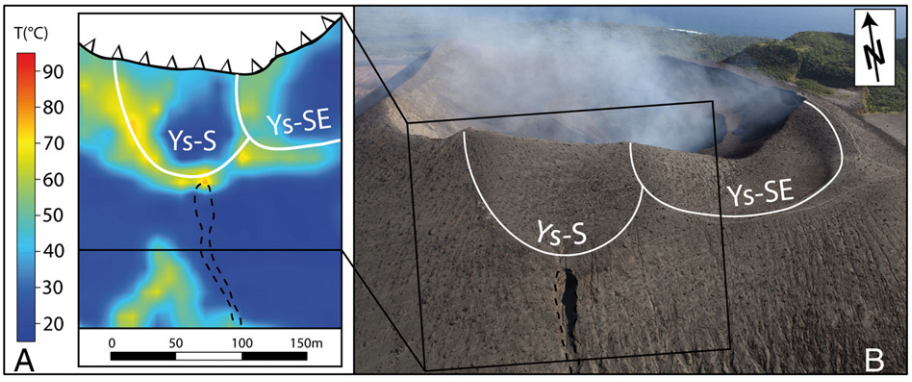

Fig. 7. Zoom on the incision zone on the southern flank of Yasur (see Fig. 2 for location of the zoom). A) Zoom on the temperature map and associated structures. B) Aerial photo of the zoom area (courtesy of Clémentine Bacri and Adrien Normier, ORA association).

much deeper than the ones of the small craters (Ys-SE, Ys-E and Ys-NE). According to this hypothesis, hydrothermal fluids rising from depth would follow the first boundary they encounter, namely the HS-N/HS-S boundary.

2) HS-S could be the hidden extension of the F-N fault toward the intersection point of linear faults below the cone, discussed above. Indeed, HS-S is in the continuity of the F-N fault, which vanishes below the cone, covered by recent tephra material.

Subsurface thermal mapping thus appears as an efficient tool to detect hidden structures in the landscape.

5.3. Impact in term of landslide hazards

Evidence of both paleo-crater rims and faults on Yasur, for some hidden in the landscape, is critical for risk assessment of flank landslides.

In the summit area, paleo-crater rims form a limit between consolidated, old material and sub-recent, loose, scoriaceous, filling material. They are concentrating fluid releases, and most probably form altered plans. They thus represent preferential flank sliding surfaces, and a threat for tourists walking in these areas. The difference in competence of material forming the old structures and recent covering tephra also drives preferential erosion paths. Paleo-crater YS-S triggered the onset of a vertical incision (Fig. 7). This latter might be activated during consequent rains, initiating lahars or even landslides. Hydrothermal paths, which are most likely argilized in depth, represent preferential zones of decoupling and initiation of cone flank destabilization, as occurred in 1975 on the northern flank (Eissen et al., 1991).

The faults, which terminations vanish below the cone, can be at the origin of large-scale destabilization of the whole cone. As suggested by Merle et al. (2001), reactivation of underlying tectonic faults in the volcano cone basement may trigger volcano flank instabilities. Similar altered fault system also affects the eastern limit of the Yenkahe block, and might lead to landslide into the ocean, with subsequent triggering of tsunamis and catastrophic impact on Tanna as well as the nearby islands.

6. Conclusion

Our study shows the presence of a complex system of heat release and hydrothermal fluid circulation below the Yasur–Yenkahe complex. Circulation, though propagating vertically as a whole, is funneled by stratification. Thus, the main thermal fluid release is almost exclusively concentrated on structural features that break the seals induced by the stratified nature of the ground. Three types of medium/high temperature anomalies have been evidenced: (1) broad hydrothermalized areas linked with planar stratification that favor lateral spreading, (2) linear segments that represent active faults, and (3) arcuate segments related to paleo-crater rims.

The limit between the Yasur volcano and the Yenkahe resurgent block is characterized by an active fault system accommodating both the rapid uplift of the Yenkahe block and the overloading induced by the volcano weight. In such a setting, faults converge below the cone of Yasur, which acts as a focus for the faults.

Argilization by hydrothermal alteration is an important factor that can develop sliding layers and lead to major movements, especially in tropical areas experiencing a rainy season. Thermal surveys, which permit to detect hydrothermal circulation paths, sometimes hidden in the landscape, are thus an important tool for hazard assessment.

Acknowledgments

This project was funded by INSU-2011-CT3-RISK project. GAD is partly funded by the Elitenetzwerk Bayern. Our fieldwork benefited from Vanuatu Meteorology and GeoHazards department. We thank Clémentine Bacri and Adrien Normier (ORA association) for the aerial photography survey of Yasur made in the framework of the project Wings for science (http://wingsforscience.com). We acknowledge Marie Chaput for providing the digital elevation model of Yasur volcano and Nicolas Villeneuve for converting the SRTM data set of the digital elevation model of Tanna island. We thank the two anonymous reviewers for their helpful comments. This is IPGP contribution n°3296.

References

Antoine, R., Baratoux, D., Rabinowicz, M., Fontaine, F., Bachèlery, P., Staudacher, T., Saracco, G., Finizola, A., 2009. Thermal infrared image analysis of a quiescent cone on Piton de la Fournaise volcano: evidence of convective air flow within an unconsolidated soil. Journal of Volcanology and Geothermal Research 183, 228–244.

Aubert de la Rue, E., 1960. Les manifestations actuelles du volcanisme aux Nouvelles Hebrides (Melanesie). Bulletin Volcanologique 23, 197–205.

Aubert, M., Baubron, J.-C., 1988. Identification of a hidden thermal fissure in a volcanic terrain using a combination of hydrothermal convection indicators and soil–atmosphere analysis. Journal of Volcanology and Geothermal Research 35, 217–225.

Aubert, M., Diliberto, S., Finizola, A., Chébli, Y., 2007. Double origin of hydrothermal convective flux variations in the Fossa of Vulcano (Italy). Bulletin of Volcanology 70, 743–751.

Barde-Cabusson, S., Finizola, A., Revil, A., Ricci, T., Piscitelli, S., Rizzo, E., Angeletti, B., Balasco, M., Bennati, L., Byrdina, S., Carzaniga, N., Crespy, A., Di Gangi, F., Morin, J., Perrone, A., Rossi, M., Roulleau, E., Susk, i B., Villeneuv, e, N., 2009. New geological insights and structural control on fluid circulation in La Fossa cone (Vulcano, Aeolian Islands, Italy). Journal of Volcanology and Geothermal Research 185, 231–245.

Carapezza, M.L., Ricci, T., Ranaldi, M., Tarchini, L., 2009. Active degassing structures of Stromboli and variations in diffuse CO2 output related to the volcanic activity. Journal of Volcanology and Geothermal Research 182 (3–4), 231–245.

Carnay, J.N., Macfarlane, A., 1979. Geology of Tanna, Aneityum, Futuna and Aniva. New Hebrides Geological Survey Report, pp. 5–29.

Chaput, M., 2009. Etude du système hydrothermal du complexe Yasur-Bloc résurgent du Yenkahe (Ile de Tanna, Vanuatu). Approche multidisciplinaire. Master report. Laboratoire Magmas et Volcans of Clermont-Ferrand and Reunion island University, France. 51 pp.

Chen, J.K., Taylor, F.W., Edwards, R.L., Cheng, H., Burr, G.S., 1995. Recent emerged reef terraces of the Yenkahe resurgent block, Tanna, Vanuatu: implications for volcanic, landslide and tsunami hazards. Journal of Geology 103, 577–590.

Chiodini, G., Cioni, R., Guidi, M., Raco, B., Marini, L., 1998. Soil CO_2 flux measurements in volcanic and geothermal areas. Applied Geochemistry 13 (5), 543–552.

Chiodini, G., Granieri, D., Avino, R., Caliro, S., Costa, A., Werner, C., 2005. Carbon dioxide diffuse degassing and estimation of heat release from volcanic and hydrothermal systems. Journal of Geophysical Research 110, B08204, http://dx.doi.org/10.1029/2004JB003542.

Delle Donne, D., Harris, A.J.L., Ripepe, M., Wright, R., 2010. Earthquake-induced thermal anomalies at active volcanoes. Geology 38 (9), 771–774.

Eissen, J.P., Blot, C., Louat, R., 1991. Chronology of the historic volcanic activity of the New Hebrides island arc from 1595 to 1991. Rapp. Sci. Tech: Sci. Terre: Géol.-Géophys., 2. ORSTOM, Nouméa. 68 pp.

Erre, C., 2005. GPS characterization of vertical movements at Yasur and Lopevi active volcanoes in Vanuatu arc. Real-time RTK-GPS measurements, INSA report, Strasbourg. 210 pp. , http://www.insa-strasbourg.fr/fr/gilbert-ferhat/index.html.

Finizola, A., Sortini, F., Lénat, J.F., Valenza, M., 2002. Fluid circulation at Stromboli volcano (Aeolian Islands, Italy) from self potential and soil gas surveys. Journal of Volcanology and Geothermal Research 116, 1–2 1–18.

Finizola, A., Sortino, F., Lénat, J.F., Aubert, M., Ripepe, M., Valenza, M., 2003. The summit hydrothermal system of Stromboli. New insights from self-potential, temperature, CO2 and fumarolic fluid measurements, Structural and monitoring implications. Bulletin of Volcanology 65, 486–504.

Finizola, A., Revil, A., Rizzo, E., Piscitelli, S., Ricci, T., Morin, J., Angeletti, B., Mocochain, L., Sortino, F., 2006. Hydrogeological insights at Stromboli volcano (Italy) from geoelectrical, temperature, and CO2 soil degassing investigations. Geophysical Research Letters 33, L17304, http://dx.doi.org/10.1029/2006GL026842.

Finizola, A., Ricci, T., Deiana, R., Barde-Cabusson, S., Rossi, M., Praticelli, N., Giocoli, A., Romano, G., Delcher, E., Suski, B., Revil, A., Menny, P., Di Gangi, F., Letort, J., Peltier, A., Villasante-Marcos, V., Douillet, G., Avard, G., Lelli, M., 2010. Adventive hydrothermal circulation on Stromboli volcano (Aeolian Islands, Italy) revealed by geophysical and geochemical approaches: implications for general fluid flow models on volcanoes. Journal of Volcanology and Geothermal Research 196, 111–119.

Gauthier, P.-J., Goff, F., Love, S., Counce, D., 2001. Geochemical surveillance of fluid and gas discharges at Yasur volcanic complex, Tanna island, Vanuatu. EUG XI General Assembly, Strasbourg, France, Abstract H6.2024. .

Harris, A.J.L., Maciejewski, A.J.H., 2000. Thermal surveys of the Vulcano Fossa fumarole field 1994–1999: evidence for fumarole migration and sealing. Journal of Volcanology and Geothermal Research 102, 119–147.

Harris, A.J.L., Ripepe, M., 2007. Regional earthquake as a trigger for enhanced volcanic activity: evidence from MODIS thermal data. Geophysical Research Letters 34, L02304, http://dx.doi.org/10.1029/2006GL028251.

Harris, A.J.L., Flynn, L.P., Dean, K., Pilger, E., Wooster, M., Okubo, C., Mouninis-Mark, P., Garbeil, H., le Cruz, De, Reyna, S., Thornber, C., Rothery, D., Wright, R., 2000. Real-time monitoring of volcanic hot spots with satellites. In: Mouginis-Mark, P., et al.

(Ed.), Remote sensing of active volcanism: American Geophysical Union Geophysical Monograph Series, 116, pp. 139–159.
Lagios, E., Vassilopoulou, S., Sakkas, V., Dietrich, V., Damiata, B.N., Ganas, A., 2007. Testing satellite and ground thermal imaging of low-temperature fumarolic fields: the dormant Nisyros Volcano (Greece). Journal of Photogrammetry and Remote Sensing 64, 447–460.
Lardy, M., Tabbagh, A., 1999. Measuring and interpreting heat fluxes from shallow volcanic bodies using vertical temperature profiles: a preliminary test. Bulletin of Volcanology 60, 441–447.
Lewicki, J.L., Connor, C., St-Amand, K., Stix, J., Spinner, W., 2003. Self-potential, soil CO2 flux, and temperature on Masaya volcano, Nicaragua. Geophysical Research Letters 30 (15), http://dx.doi.org/10.1029/2003GL017731 ISSN: 0094–8276.
Louat, R., Hamburger, M., Monzier, M., 1988. Shallow and intermediate-depth seismicity in the New Hebrides arc: constraints on the subduction process. In: Greene, H.G., Wong, F.L. (Eds.), Geology and offshore resources of Pacific Island Arcs, Vanuatu Region. : Earth Sci. Ser., 8. Circum-Pac. Counc. Energy Miner. Resour., Houston, Tex., pp. 329–356.
Merle, O., Vidal, N., van Wyk de Vries, B., 2001. Experiments on vertical basement fault reactivation below volcanoes. Journal of Geophysical Research 106 (B2), 2153–2162.
Metrich, N., Allard, P., Aiuppa, A., Bani, P., Bertagnini, A., Shinohara, H., Parello, F., Di Muro, A., Garaebiti, E., Belhadj, O., Massare, D., 2011. Magma and volatile supply to post-collapse volcanism and block resurgence in Siwi caldera (Tanna island, Vanuatu arc). Journal of Petrology 52, 1077–1105.
Murphy, S.W., Souza Filho, C.R., Oppenheimer, C., 2011. Monitoring volcanic thermal anomalies from space: size matters. Journal of Volcanology and Geothermal Research 203, 48–61.
Nairn, I.A., Scott, B.J., Giggenbach, W.F., 1988. Yasur volcanic investigations, Vanuatu September 1988. New Zealand Geological Survey Report, pp. 1–74.
Neef, G., Zhao, J.X., Collerson, K.D., Zhang, F.S., 2003. Late Quaternary uplift and subsidence of the west coast of Tanna, south Vanuatu, southwest Pacific: U – Th ages from the raised coral reefs in the median sedimentary basin. Australian Journal of Earth Sciences 50, 39–48.
Otto, G.H., 1939. A modified logarithmic probability graph for the interpretation of mechanical analysis of sediments. Journal of Sedimentary Petrology 9, 62–76.
Pergola, N., Marchese, F., Tramutoli, V., 2004. Automated detection of thermal features of active volcanoes by means of infrared AVHRR records. Remote Sensing of Environment 93, 311–327.
Revil, A., Finizola, A., Sortino, F., Ripepe, M., 2004. Geophysical investigations at Stromboli volcano, Italy. Implications for ground water flow and paroxysmal activity. Geophysical Journal International 157, 426–440.
Revil, A., Finizola, A., Piscitelli, S., Rizzo, E., Ricci, T., Crespy, A., Angeletti, B., Balasco, M., Barde-Cabusson, S., Bennati, L., Bolève, A., Byrdina, S., Carzaniga, N., Di Gangi, F., Morin, J., Perrone, A., Rossi, M., Roulleau, E., Suski, B., 2008. Inner structure of La Fossa di Vulcano (Vulcano Island, southern Tyrrhenian Sea, Italy) revealed by high resolution electric resistivity tomography coupled with self-potential, temperature, and CO2 diffuse degassing measurements. Journal of Geophysical Research 113, B07207, http://dx.doi.org/10.1029/2007JB005394.
Revil, A., Finizola, A., Ricc, i, T., Delcher, E., Peltier, A., Avard, G., Bailly, T., Barde-Cabusson, S., Bennati, L., Byrdina, S., Colonge, J., Di Gangi, F., Douillet, G., Lupi, M., Letort, J., Tsang Hin Sun, E., 2011. Hydrogeology of Stromboli volcano, Aeolian Islands (Italy) from the interpretation of resistivity tomograms, self-potential, soil temperature, and soil CO2 concentration measurements. Geophysical Journal International 186, 1078–1094.
Rubin, A.M., Pollard, D.D., 1988. Dike-induced faulting in rift zones of Iceland and Afar. Geology 16, 413–417.
Schöpa, A., Pantaleo, M., Walter, T.R., 2011. Scale-dependent location of hydrothermal vents: stress field models and infrared field observations on the Fossa Cone, Vulcano Island, Italy. Journal of Volcanology and Geothermal Research 203, 133–145.
Sinclair, A.J., 1974. Selection of threshold values in geochemical data using probability graphs. Journal of Geochemical Exploration 3, 129–149.
Staudacher, T., 2010. Field observations of the 2008 summit eruption at Piton de la Fournaise (Ile de La Réunion) and implications for the 2007 Dolomieu collapse. Journal of Volcanology and Geothermal Research 191, 60–68.
Steel, R.S., 1880. The New Hebrides and Christian Missions. James Nisbet and Co., London, pp. 420–430.
Taylor, F.W., Mann, P., Bevis, M.G., Edwards, R.L., Cheng, H., Cutler, K.B., Gray, S.C., Burr, G.S., Beck, J.W., Phillips, D.A., Cabioch, G., Recy, J., 2005. Rapid forearc uplift and subsidence caused by impinging bathymetric features: examples from the New Hebrides and Solomonarcs. Tectonics 24 (6), TC6005.
vanWyk de Vries, B., Merle, O., 1996. The effect of volcanic constructs on rift fault pattern. Geology 24 (7), 643–646.
vanWyk de Vries, B., Merle, O., 1998. Extension induced by volcanic loading in regional strike-slip zones. Geology 26 (11), 983–986.